JOURNAL OF GEOPHYSICAL RESEARCH: EARTH SURFACE, VOL. 118, 1–11, doi:10.1002/jgrf.20052, 2013

The effects of entrained debris on the basal sliding stability of a glacier

L. K. Zoet,[1,2] B. Carpenter,[3] M. Scuderi,[1] R. B. Alley,[1] S. Anandakrishnan,[1] C. Marone,[1] and M. Jackson[4]

Received 23 October 2012; revised 12 February 2013; accepted 25 February 2013.

[1] New laboratory experiments exploring likely subglacial conditions reveal controls on the transition between stable sliding and stick-slip motion of debris-laden ice over rock, with implications for glacier behavior. Friction between a rock substrate and clasts in ice generates heat, which melts nearby ice to produce lubricating water. An increase in sliding speed or an increase in entrained debris raises heat generation and thus meltwater production. Unstable sliding is favored by low initial lubrication followed by rapid meltwater production in response to a velocity increase. Low initial lubrication can result from cold or drained conditions, whereas rapid increase in meltwater generation results from strong frictional heating caused by high sliding velocity or high debris loads. Strengthening of the interface (healing) during "stick" intervals between slip events occurs primarily through meltwater refreezing. When healing and unstable sliding are taken together, the experiments reported here suggest that stick-slip behavior is common from motion of debris-laden glacier ice over bedrock.

Citation: Zoet, L. K., B. Carpenter, M. Scuderi, R. B. Alley, S. Anandakrishnan, C. Marone, and M. Jackson (2013), The effects of entrained debris on the basal sliding stability of a glacier, *J. Geophys. Earth Surf.*, *118*, doi:10.1002/jgrf.20052.

1. Introduction

[2] Glaciers and ice sheets often generate seismic events [*West et al.*, 2010; *Anandakrishnan and Alley*, 1997a; *Weaver and Malone*, 1979; *Danesi et al.*, 2007; *Zoet et al.*, 2012], through processes including surface crevassing [*Neave and Savage*, 1970], calving at the terminus [*Ekstrom et al.*, 2006; *O'Neel et al.*, 2010], and outburst flooding [*Winberry et al.*, 2009a]. Many events are caused by sudden slip in the ice-flow direction on planes that are indistinguishable from the glacier bed, within the ∼10 m depth uncertainty [*Smith*, 2006; *Stuart et al.*, 2005; *Anandakrishnan and Alley*, 1997b; *Anandakrishnan and Bentley*, 1993; *Walter et al.*, 2011; *Winberry et al.*, 2009b]. Current knowledge of subglacial mechanics suggests that the seismic events arise from sliding of debris-rich ice over bedrock [*Alley*, 1993], although ruptures within overriding ice or within subglacial material cannot be completely ruled out. Basal ice, often up to several meters thick and containing debris loads up to 40% by volume [*Kirkenbride*, 2002], slides over material ranging from crystalline bedrock to water saturated till [*Peters et al.*, 2006; *Smith*, 2006; *Tulaczyk et al.*, 2000; *Blankenship et al.*, 1986]. Geological field studies [*Fischer and Clarke*, 1997; *Iverson et al.*, 2003] and geophysical data provide insights into basal sliding processes [*Anandakrishnan and Alley*, 1997a, b], and laboratory observations can supplement and extend the sparse field data on glacier-bed seismicity.

[3] Field geodetic and direct observations show that glacier flow can be smooth or stick-slip, with variations over time [*Hubbard*, 2002; *Winberry et al*., 2009a, b; *Wiens et al*., 2008; *Zoet et al*., 2012] and space at various scales [*Wiens et al.*, 2008; *Winberry et al.*, 2009b; *Anandakrishnan and Bentley*, 1993; *Anandakrishnan and Alley*, 1994]. Tides, variable meltwater input, calving, and variations in basal debris load are among the processes that can affect motion and thus seismicity [*Anandakrishnan and Alley*, 1997b; *Walter et al*., 2008; *Christianson*, 2012; *Fischer and Clarke*, 1997; *Nettles et al*., 2008; *Zoet et al*., 2012].

[4] The sliding interface at the base of a glacier shares key characteristics with tectonic fault zones. Unstable sliding in such fault zones results from a dynamic frictional instability attendant with local stress drop and seismic radiation [*Scholz*, 2002]. As stress is recharged at the fault interface, due to tectonic loading in the case of earthquake faults, or basal glacial flow, a repetitive stick-slip pattern may emerge. Recent work shows that both fault and subglacial slip exhibit a spectrum of behavior, ranging from creep through transient slow slip to dynamic earthquake rupture [*Rignot et al.*, 2011; *Winberry et al.*, 2009a; *Zoet et al.*, 2012]. Data on stable or unstable sliding and subsequent stress recharge are often interpreted within the framework of rate-and-state dependent friction laws (RSF)

[1]Department of Geoscience, Penn State University, University Park, Pennsylvania, USA.
[2]Now at Department of Geologic and Atmospheric Sciences, Iowa State University, Ames, Iowa, USA.
[3]HP-HT Lab, Istituto Nazionale di Geofisica e Vulcanologia, Rome, Italy.
[4]Hydrology Department Norwegian Water Resources and Energy Directorate, Oslo, Norway.

Corresponding author: L. K. Zoet, Department of Geologic and Atmospheric Sciences, Iowa State University, 362 Science 1, Ames, IA, 50011, USA. (lzoet@iastate.edu)

2169-9003/13/10.1002/jgrf.20052

[*Dieterich*, 1979a; *Ruina*, 1983; *Scholz*, 1998]. RSF analysis has been used extensively in earthquake studies [*Marone*, 1998a; *Scholz*, 1998; *Carpenter et al.*, 2011], but much less commonly in cryospheric studies [e.g., *Rathbun et al*., 2008; *Fortt and Schulson*, 2009].

[5] In this paper, we present results on the frictional constitutive properties of debris-bearing and clean glacial ice from experiments conducted in a laboratory setting. We focus in particular on the frictional strength, sliding stability, and processes of frictional restrengthening (so-called frictional healing) following stick-slip failure events in glaciological settings. We describe a series of laboratory shearing experiments conducted on natural and synthetic glacial ice with a range of debris contents (0–50% by weight) and at a temperature range from –6°C to the pressure melting point (pmp). Applied stresses and other experimental conditions were chosen to be representative of subglacial conditions.

1.1. Friction Constitutive Laws for Seismic and Aseismic Glacial Sliding

[6] The rate-state friction laws [*Dieterich*, 1979a, 1979b; *Ruina*, 1983; *Rice*, 1983] describe time- and slip-dependent changes in frictional strength, and have been used extensively to describe a range of seismic and aseismic slip behavior on tectonic faults [*Marone*, 1998a; *Scholz*, 1998; *Rubin*, 2011]. In the context of RSF, fault slip events during the seismic cycle, are described by variations in the frictional strength, μ, with slip velocity, V, and a state variable, θ:

$$\mu = \mu(V,\theta) = \mu_0 + a\, ln\left(\frac{V}{V_0}\right) + b\left(\frac{V_0\theta}{D_c}\right) \quad (1)$$

$$\dot{\theta} = -\left(\frac{V\theta}{D_c}\right) ln\left(\frac{V\theta}{D_c}\right) \quad (2)$$

where μ_0 is a reference friction coefficient at a reference slip velocity, V_0, V is the fault slip velocity, a and b are dimensionless empirical constants, and D_c is the critical slip distance. D_c is the *e*-folding slip distance necessary to renew the asperity contacts after a velocity perturbation, and has been related to the size of frictional contact junctions [e.g., *Rabinowicz*, 1951; *Dieterich*, 1979a; 1981], or the porosity, or width of shear localization bands [*Marone and Kilgore*, 1993; *Marone et al.*, 2009]. θ is a state variable that describes the nature of the area of contact at a given time. *Dieterich* [1979a] suggested that the state variable can be interpreted as the average life time of the contacts. Equation (1) describes the relationship between friction, velocity and state. Equation (2) describes the evolution of state with slip and time following a slip perturbation. RSF laws have been generalized to account for changes in normal stress, variable shear localization dimension, and other variables [*Marone*, 1998a], but we focus here on the basic form of the laws.

[7] The RSF parameter a is a measure of the initial change in the friction coefficient that results from a sudden change in sliding velocity, and b represents the evolution of the friction coefficient with slip following a perturbation [*Marone*, 1998a]. The parameter $a - b$ represents the change in steady-state friction with slip velocity, with positive values indicating so-called velocity-strengthening behavior and negative values representing velocity-weakening behavior. The stability of frictional slip is determined, to first order, by the ratio of $b - a$ over D_c [*Rice*, 1983]. Velocity-strengthening friction produces only stable frictional sliding, whereas velocity-weakening friction can produce unstable sliding and thus stick-slip behavior.

[8] From rate-and-state friction theory, in the velocity strengthening regime where steady-state friction increases with sliding velocity, faster sliding on an interface requires more work, which requires higher driving stress and thus tends to damp velocity perturbations in response to stress perturbations. This effect combines with atomic-scaled processes to ensure that the friction direct effect a is positive [e.g., *Marone*, 1998a; *Beeler et al*., 2008; *Li et al*., 2011]. The friction evolution effect b describes the extent to which contact junctions evolve with slip and time following a perturbation from steady state. For extended solid surfaces, the average asperity contact lifetime is given by the ratio of contact junction dimension divided by slip velocity. Under conditions of velocity weakening friction, where steady-state friction decreases with sliding velocity, contact junction size decreases with increasing slip velocity because at the higher slip rate, contacts are smaller and/or composed of weaker chemical bonds. Other effects such as increased lubrication or asperity breakage can further weaken the interface. Such rate-and-state dependent friction processes lead to velocity-strengthening and velocity-weakening of an interface, and are represented by a and b, respectively. The sign of the difference $a - b$ determines whether the interface as a whole is velocity-strengthening and slides stably, or velocity-weakening, which is a necessary condition for stick-slip instabilities.

[9] In the context of glacial slip, RSF describes variations in frictional strength of the interface between ice and its underlying rock or sediment layer. The strength of that interface changes with changes in the population and lubrication of contacts through breakage, melting or other processes. During the pre-seismic ("stick") phase of the seismic cycle, the strength of the shearing ice/debris zone increases with time at a rate that can be described by RSF laws. The rate of frictional restrengthening (frictional healing) is governed by time, shear stress, and loading velocity [e.g., *Karner and Marone*, 2001]. Frictional healing results from processes such as creep-induced growth of the contact area [*Dieterich and Kilgore*, 1994], porosity loss and densification, and strengthening of chemical bonds within highly-stressed contact junctions [*Li et al.*, 2011]. Many of these processes vary strongly with temperature, and in subglacial environments, freezing of lubricating meltwater is likely to play a role in frictional healing of debris-laden ice on bedrock [*Robin*, 1976; *Goodman et al.*, 1979]. Ice also may strengthen through re-entrainment of debris melted out during a slip event, through regelation and freeze-on processes. Such strengthening can contribute to stick-slip behavior [*Zoet et al.*, 2012]. The parameter β is used to quantify the rate at which these frictional healing mechanisms occur, and is estimated through slide-hold-slide testing (detailed later in this paper).

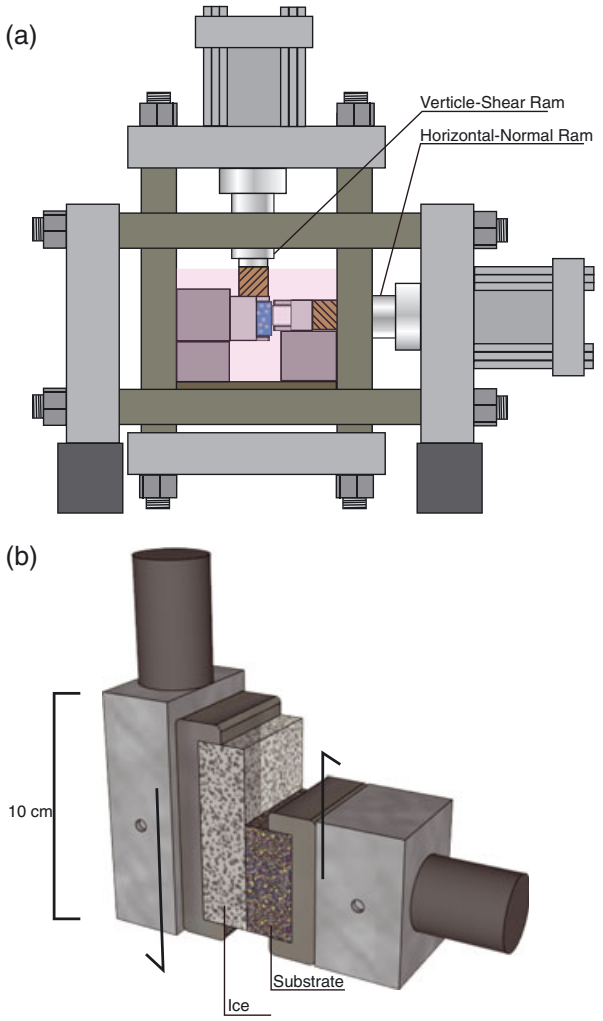

Figure 1. (a) Biaxial shearing apparatus. Area in pink is cooled to a target temperature and thermally insulated. Normal stress is applied with the horizontal ram while shear stress is applied with the vertical ram. (b) Sample grip assembly. Left loading platen carries the debris-rich ice block, which is sheared past the rock sample (Westerly Granite), held by the right platen. This setup allows for 25 mm of displacement.

2. Methods

[10] Our experiments were conducted in a servo-controlled biaxial testing apparatus using a modified double-direct shear configuration. Sliding interfaces were debris-laden ice sheared over rock surfaces (westerly granite), and were designed to reproduce key features at the base of a glacier moving over subjacent bedrock (Figure 1). We studied ice with debris contents ranging from 0–50% by weight (0–26% by volume), and at temperatures ranging from –6°C to the pressure melting point (pmp). The sample assembly was thermally isolated, and temperature was carefully controlled and monitored throughout all tests. Experiments were conducted following standard procedures that have been developed for a variety of materials and rock types in the study of fault mechanics [*Marone*, 1998a; *Ikari et al.*, 2009; *Carpenter et al.*, 2011].

[11] Samples of ice were held in a specially designed loading platen and subjected to direct shear against a rock surface in a modified double-direct shear configuration (Figure 1). Experiments were conducted at constant normal stress, in the range 0.5–1.25 MPa (the main experiments listed in Table 1 were all run at 1.25 MPa), which was chosen to simulate the weight of the glacier (140 m of ice) on its bed. The drained experimental system prevents water pressure buildup at the interface, and so produces an effective pressure similar to that for a well-drained 140 m-thick glacier. Effective pressure is important in controlling subglacial friction [*Cuffey and Paterson*, 2010]. Normal stress was maintained at a constant value using a fast-acting hydraulic servo controller with feedback from custom made load cell and calibrated to NBS standards. Normal and shear forces are accurate to ± 5 N and measured with precision of 5 N. Shear and normal displacement were measured to $\pm$ 0.1 μm using direct-current displacement transducers (DCDT) mounted directly on the loading rams. Samples were sheared by driving the vertical loading ram at constant velocity (Figure 1). A maximum shear displacement of 25 mm is attainable in this configuration. All data were recorded with a 24 bit digitizer operating at 10 kHz, with data averaged and saved at a rate from 1–1000 Hz, depending on imposed sliding velocity.

[12] We constructed ice samples that contained 0–50% debris by weight to represent basal ice with varying debris loads. Where access to basal ice has been available [*Kirkenbride*, 2002], basal debris loads of 0–40% by volume (0–68% by weight) have been observed. The samples were constructed after the model of *Emerson and Rempel* [2007].

[13] We used both natural and simulated glacial debris. Debris was chosen with a bimodal (Figure 2) particle-size distribution to replicate typical debris entrained in basal ice [*Kirkenbride*, 2002]. The particular debris used consisted primarily of amphibole schist, appropriate for glaciation over a crystalline bedrock. Debris grains larger than 1.25 mm ($\sim \frac{1}{10}$ of the minimum dimension) were removed, following the standard convention in soil testing.

[14] Preparation of the samples consisted of crushing debris-free ice until no grains larger than 2 mm in diameter remained. Ice grains were then placed in a container with a known debris mass, and the debris-ice mixture was agitated until all debris uniformly coated the ice grains. The mixture was then placed in a $4.5 \times 7.0 \times 1.0$ cm mold, matching the loading platen used in the testing machine (Figure 1). Water near 0°C was used to flood the mold, fixing the debris in its random distribution throughout the sample block. Water close to 0°C was preferable so as to keep refreezing time to a minimum and to preserve the random distribution of the debris. The water used for both the initial seed ice and the mold flooding was filtered and de-aerated to minimize any effect of bubbles or impurities.

[15] For most experiments, a block of Westerly Granite ($4.5 \times 5.0 \times 1.0$ cm) was used to simulate the bedrock in contact with the debris-rich ice. The granite block was milled flat on a surface grinder, and had no more than a 4×10^{-4} slope to the face. After grinding, the granite surface was polished with a 60 grit silicon-carbide polishing compound to produce a uniform roughness of $\sim$ 15 μm RMS. In the center of the granite block, we drilled a 3 mm diameter hole perpendicular to the sliding surface to accommodate a glass

Table 1. Experiment Parameters

Experiment	% Deb.	Normal (MPa)	Velocities (μm / s)	Holds (s)	Temp C	Shear Mat.
p2844	40	1.25	10-3-30-300	10-30-100-300	–6	WG
p2845	50	1.25	10-3-30-300	10-30-100-300	–6	WG
p3141	10	1.25	10-3-10-30-60-100-300	3-10-30-100-300	–6	WG
p3142	10	1.25	10-3-10-30-60-100-300	3-10-30-100-300	–6	WG
p3143	20	1.25	10-3-10-30-60-100-300	3-10-30-100-300	–6	WG
p3144	30	1.25	10-3-10-30-60-100-300	3-10-30-100-300	–6	WG
p3145	50	1.25	10-3-10-30-60-100-300	3-10-30-100-300	–6	WG
p3146	5	1.25	10-3-10-30-60-100-300	3-10-30-100-300	–6	WG
p3562	20	1.25	10-3-10-30-60-100-300	1-3-10-30-100	pmp	WG
p3563	5	1.25	10-3-10-30-60-100-300	1-3-10-30-100	pmp	WG
p3564	10	1.25	10-3-10-30-60-100-300	1-3-10-30-100	pmp	WG
p3565	20	1.25	10-3-10-30-60-100-300	1-3-10-30-100	pmp	WG
p3566	30	1.25	10-3-10-30-60-100-300	1-3-10-30-100	pmp	WG
p3567	40	1.25	10-3-10-30-60-100-300	1-3-10-30-100	pmp	WG
p3568	50	1.25	10-3-10-30-60-100-300	1-3-10-30-100	pmp	WG
p3589	20	1.25	10-3-10-30-60-100-300	1-3-10-30-100	–3	WG
p3590	40	1.25	10-3-10-30-60-100-300	1-3-10-30-100	–3	WG
p3591	20	1.25	10-3-10-30-60-100-300	1-3-10-30-100	–3	WG
p3593	50	1.25	10-3-10-30-60-100-300	1-3-10-30-100	–3	WG
p3594	10	1.25	10-3-10-30-60-100-300	1-3-10-30-100	–3	WG
p3595	30	1.25	10-3-10-30-60-100-300	1-3-10-30-100	–3	WG
p3596	50	1.25	3-10-60-3-10-60-3-10-60	-	–3 to pmp	WG
p3628	37	1.25	10-3-10-30-60-100-300	1-3-10-30-100	pmp	BS
p3739	0	1.25	10	1-3-10-30-100	–3	WG
p3740	0	1.25	10	1-3-10-30-100	–6	WG
p3741	0	1.25	10	1-3-10-30-100	pmp	WG
p3742	0	1.25	10	1-3-10-30-100	–3	WG

* WG is Westerly Granite; BS is Berea Sandstone

bead thermistor, which was mounted flush to the surface to record temperatures at the sliding interface. The granite is nearly impermeable (permeability of $\sim 10^{-21}$ m^2) and therefore a few experiments were conducted using a highly permeable Berea sandstone (permeability $\sim 10^{-14}$ m^2) as the bedrock base.

[16] Two glass-bead thermistors (YSI 55000 Series GEM Glass Thermistors) were used to record temperatures: one at the sliding interface in the granite block, and a second

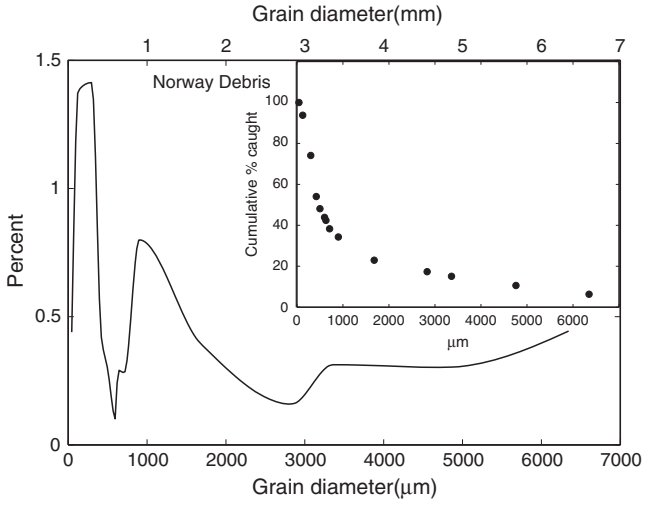

Figure 2. Glacial debris particle size distribution. Main panel shows percentage of debris for each sieve size. Inset shows cumulative debris percentage. Note bimodal nature of the distribution.

(on most experiments) within the ice during the sliding experiment. A ratiometric half-bridge circuit, with an operational amplifier for gain, was used in conjunction with a 24 bit digitizer unit to record temperatures with accuracy of 0.1°C. With further calibration, greater accuracies have been achieved using these units, but we found that 0.1°C precision was adequate for our experiments [*Iverson and Petersen*, 2011].

[17] Processes involving ice deformation and premelting are especially sensitive to temperature changes near the bulk melting point [e.g., *Cuffey and Paterson*, 2010], so temperature control was important for reproducibility of results. To maintain a constant temperature, we wrapped the internal portion of the testing apparatus, including the steel alignment blocks and the loading platens, in insulation. The steel alignment blocks were separated from the remainder of the frame by acrylic plates with low thermal conductivity (0.2 W (m C)$^{-1}$), effectively isolating every component within the insulated area from the outer frame. The steel alignment blocks have a large thermal mass and were chilled to the desired operating temperature before the experiment began. The short duration of each experiment ($\sim$20 min), in combination with the thermal mass of the system and insulation, kept the ice/rock interface temperatures within ± 0.5°C of the target temperature for all data reported here.

[18] A standard suite of velocity-stepping experiments as well as slide-hold-slide experiments [i.e., *Marone*, 1998a] was conducted on all debris loads and over three different temperatures (–6 °C, –3 °C, pmp). A normal stress of 1.25 MPa was applied, equal to the stress of a glacier $\sim$140 m thick with no basal water pressure, or a thicker glacier with basal water pressure 1.25 MPa less than overburden pressure. Our standard experimental procedure

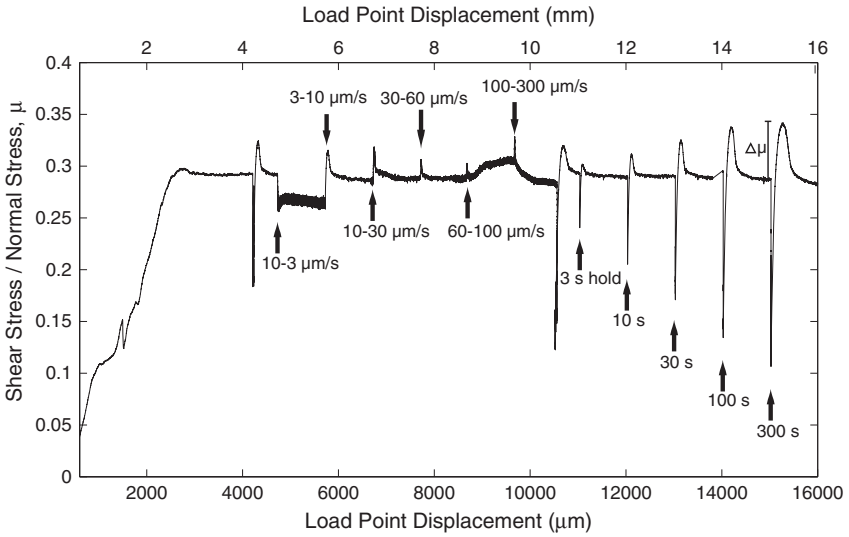

Figure 3. Friction displacement curve for a complete experiment. Initial loading is conducted at constant load point velocity of 10 μm s^{-1}, until steady-state friction is achieved. This is followed by a series of velocity stepping experiments, covering the range from 3 to 300 μm s^{-1}, and slide-hold-slide experiments. Hold times range from 3 to 300 s and we measure frictional healing ($\Delta\mu$) as the change in peak friction following the hold period relative to the initial value of sliding friction. Steady state sliding friction increases with velocity, indicating velocity-strengthening behavior, at low velocity, and transitions to velocity-weakening behavior at the highest velocities.

(Figure 3) consisted of a ∼3 mm run-in at a constant velocity of 10 μm s^{-1}, until a steady-state friction coefficient was achieved. Subsequently, velocity was increased stepwise from 3 to 300 μm s^{-1} with a constant shear displacement of 2 mm for each step. RSF parameters a, b, and D_c were modeled for each step, initially constrained by forward modeling and refined by a least-squares inverse technique following *Marone* [1998b]; *Blanpied et al.* [1998]. After the velocity steps, slide-hold-slide steps were performed to estimate the frictional healing rate (β). The loading velocity was 10 μm s^{-1}, and we imposed a slip displacement of 1 mm between each hold period, which ranged from 3, 10, 30, 100, and 300 s.

[19] Our primary suite of experiments using synthetic samples was augmented with a suite of tests using natural glacial ice. Basal-ice samples were taken from Engabreen Glacier in Norway, through access provided by the Svartisen subglacial laboratory, and returned frozen to our laboratory at Penn State. Each sample was divided in two, with one half used in the shear apparatus, and the other half melted to extract the entrained debris, which we used to make a synthetic-ice sample for comparison.

[20] Natural ice samples include features such as non-random c-axis fabric, debris-alignment and foliation that reflect the flow history. Comparison of results for experiments on natural and synthetic samples, constructed using the same debris, allowed an opportunity to evaluate the relative importance of these features. We cut natural ice samples parallel to the bed of the glacier and inline with the local flow direction. The laboratory samples were cut and constructed so that shear occurred in the in situ orientation and consistent with the natural flow orientation. Both the natural and the synthetic samples were subject to our standard friction testing protocol, including velocity step tests and slide-hold-slide tests as described above.

3. Results

3.1. Friction

[21] All experiments began with an initial run-in at 10 μm s^{-1} to achieve steady-state friction coefficient, μ, (Figure 3). The stable sliding friction coefficient (μ_{ss}) generally reached a constant value after 3 to 4 mm of displacement, and we measured steady-state friction coefficient at a displacement of 4 mm (Figure 4). Friction coefficient values range from

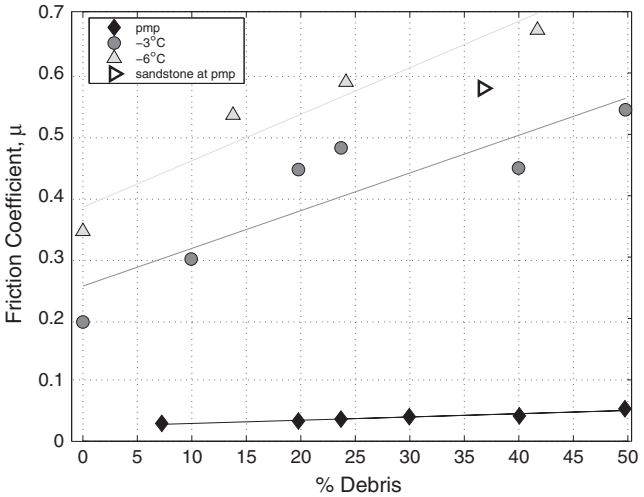

Figure 4. Steady-state coefficient of sliding friction for ice sliding against Westerly granite as a function of debris concentration in the ice at three temperatures. Friction values are taken at 10 μm s^{-1}, prior to starting the velocity step tests (see Figure 3). Note that the friction of ice sliding against Berea sandstone differs from data for ice sliding against Westerly Granite.

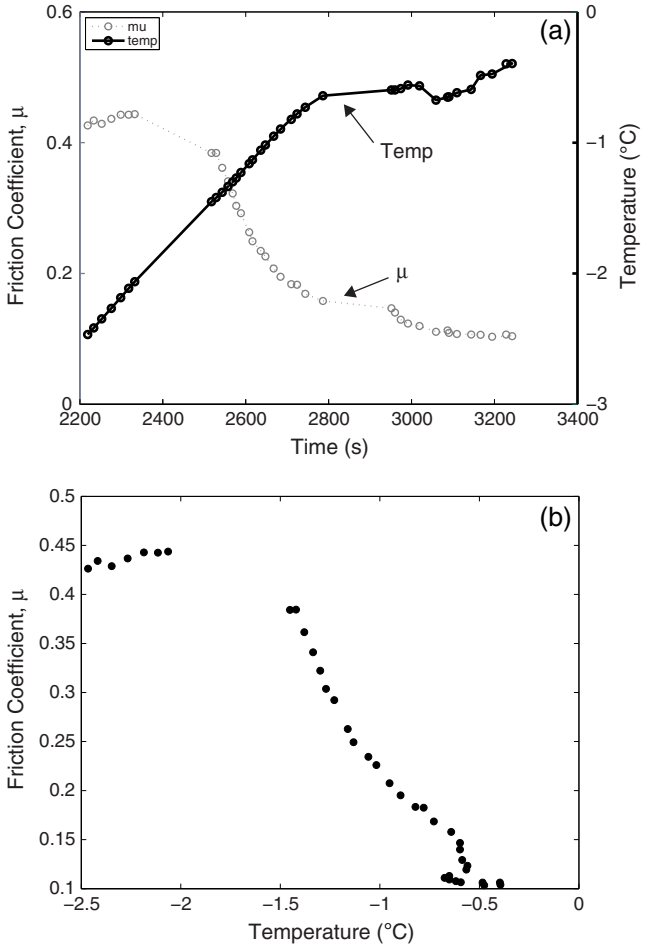

Figure 5. Sliding friction and temperature as a function of time for a complete run in which temperature was varied during shearing at 10 μm s^{-1}. (a) Note that warming induces weakening. Friction decreases from 0.4 at –2.5°C to 0.1 at –0.5°C. (b) Relationship between friction and temperature for the data shown in Figure 5a. Friction is relatively constant from –2.5 to –1.5°C, but weakens significantly as temperature rises above –1.5°C.

< 0.1 for pure ice up to nearly 0.7 for the coldest conditions (–6°C) and the highest debris concentrations (40% by weight). For each temperature, friction of pure ice on rock is lowest, and the friction coefficient increases, approximately linearly with debris concentration, by up to 0.01 per % of increase in debris concentration.

[22] We explored the role of temperature variation during a shearing experiment on a sample with 50% debris concentration (Figure 5). This sample began shearing at –2.5°C and it was allowed to warm during the initial run-in. Temperature increased to –0.5°C and, at that point, we stopped heating. Initially, the friction coefficient was relatively constant as temperature rose. The friction coefficient then decreased slowly with additional heating; the lag presumably arose as a result of thermal mass and heating of the loading platens and the sample assembly. After temperature reached –1.5°C, friction decreased rapidly, dropping from ∼0.4 to 0.1 over a 1°C warming (Figure 5b). Figure 5b shows details of the relationship between the friction coefficient and temperature in this experiment.

[23] The friction coefficient is especially low for experiments at the pmp (Figure 4). Because the temperature is high in these experiments, frictional heat generated by shearing is consumed by latent heat of melting rather than sensible heating of the ice. This suggests the hypothesis that the low friction coefficient we observe at the pmp arises from lubrication via production and accumulation of meltwater at the sliding interface. Meltwater between clasts and substrate supports a portion of the normal load otherwise carried by the debris but not the shear load, thus lowering the friction coefficient [*Bowden and Tabor*, 2001].

[24] To test this hypothesis, an additional experiment was run at the pmp with a relatively high debris concentration of 37%, favoring meltwater generation, but with a permeable Berea Sandstone substrate to allow excess meltwater to drain away. This drained pmp experiment had a friction coefficient comparable to colder runs, and much higher than pmp runs on nearly impermeable Westerly Granite (Figure 4).

3.2. Frictional Healing

[25] Slide-hold-slide results demonstrate notable strengthening with time in every instance (Figure 6). These tests

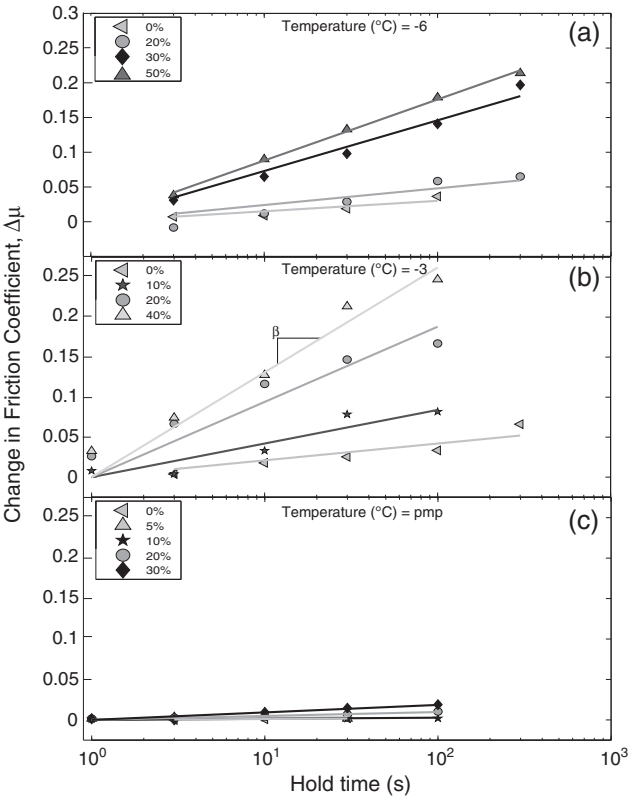

Figure 6. Results of slide-hold-slide experiments. Frictional healing parameter ($\Delta\mu$) is the increase in peak friction relative to the starting value of sliding friction (see Figure 3). Frictional healing increases systematically with hold time and debris concentration. Lines show log-linear best fits to data, and define the frictional healing rate, β. The highest values of β occur at –3°C. Ice near the pressure melting point (pmp) has much lower β than at lower temperature. All data are plotted for runs at that temperature ±0.5°C.

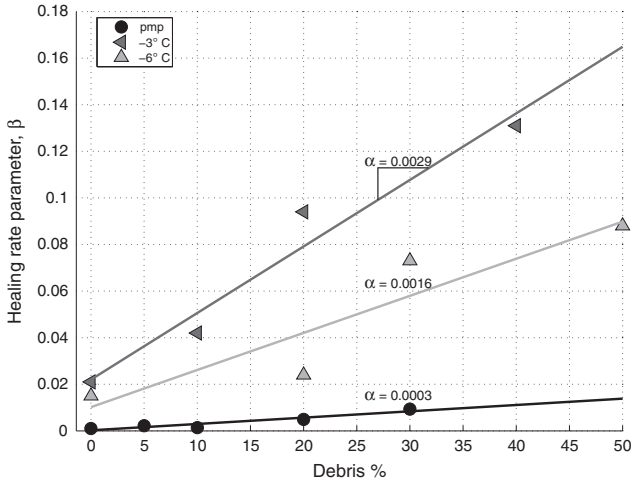

Figure 7. Variation of the frictional healing rate β as a function of temperature and debris concentration. Healing rate increases systematically with increasing debris concentration at each temperature as represented by the slope α. The temperature dependence of healing rate is more complex, with the highest values of β occurring at –3°C and the lowest values at the pmp.

were preceded by a run-in and velocity-step tests, and thus the friction coefficient had reached steady-state (Figure 3). We conducted slide-hold-slide tests by stopping the vertical loading ram for prescribed time intervals, and then continuing loading at the initial rate (10 μm s^{-1}.). The healing parameter $\Delta\mu$ is the increase in peak friction coefficient relative to the initial value of sliding friction coefficient. We find that $\Delta\mu$ increases approximately linearly with log hold time, consistent with previous work [*Dieterich*, 1978; *Beeler et al.*, 1994; *Marone*, 1998a]. For a given temperature, the healing rate $\beta = \frac{\Delta\mu}{\log(t_h)}$ increases with debris concentration (Figure 6).

[26] Figure 7 shows the dependence of β on debris concentration for each temperature, where α is the slope for a linear best fit to the data for each temperature. As expected from the data of Figure 6, the largest healing rates occur for the highest debris concentrations. However, for ice with >40% debris, the largest healing rates occur for ice at –3°C (Figure 7). The measured healing rates are lower for ice at –6°C and substantially lower for ice at the pmp.

3.3. Friction Rate Dependence

[27] Velocity stepping tests indicate stable sliding (velocity-strengthening; $a - b > 0$) at low velocities and debris loads. Increasing the driving velocity causes a transition to unstable sliding (velocity-weakening behavior; $a - b < 0$) for the subfreezing experiments (Figure 8). This transition happens at lower velocity for the warmer (–3°C) subfreezing experiments than for the colder (–6°C) tests.

[28] The transition to unstable sliding generally occurs at a lower velocity in ice that contains more debris, which favors initially higher friction and greater meltwater generation. At velocities much higher or much lower than the transition, the magnitude of $a - b$ is larger for the colder samples (note the different ordinate scales in Figure 8).

[29] All of the pmp experiments with Westerly Granite exhibit both a very low friction coefficient at run-in, and stable sliding. However, the drained pmp experiment using Berea Sandstone, with its higher run-in friction coefficient, transitioned to unstable sliding at the highest driving velocity tested to produce the most negative $a - b$ value of the experiments conducted (not shown on plots).

[30] The transition from stable to unstable sliding occurs at velocities ranging from < 30 to > 100 μm s^{-1}. For comparison, 30 μm s^{-1} ≈ 1000 m yr^{-1}, which falls within the range of natural glaciers.

3.4. Synthetic Compared with Natural Ice

[31] Natural samples from Engabreen (16% by weight) exhibit velocity dependence behavior quite similar to synthetic samples (Figure 9). However, healing is somewhat lower in the natural samples than the synthetic ones (Figure 9).

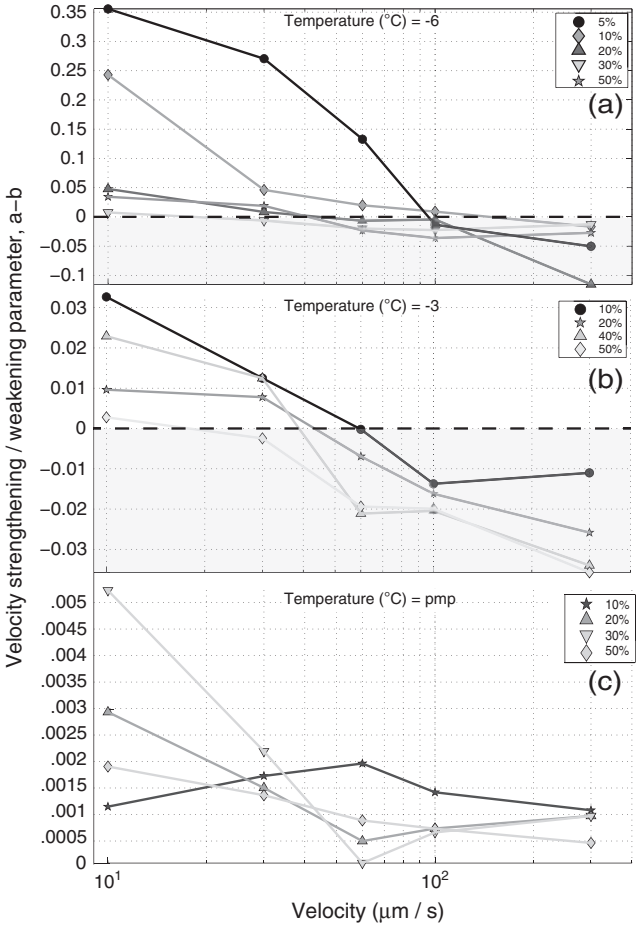

Figure 8. Results of velocity-stepping experiments showing systematic variation in $a - b$ as a function of debris concentration for temperatures of (a) –6°C (b) –3°C and (c) the pmp of ice. At the lowest velocities, friction exhibits velocity strengthening behavior for each temperature. For the two lowest temperatures, frictional behavior switches from velocity strengthening to velocity weakening as slip velocity increase. The transition velocity varies with ice debris content, but is generally in the range 30–100 μm s^{-1}. Note that 1000 m yr^{-1} ≈ 30 μm s^{-1}.

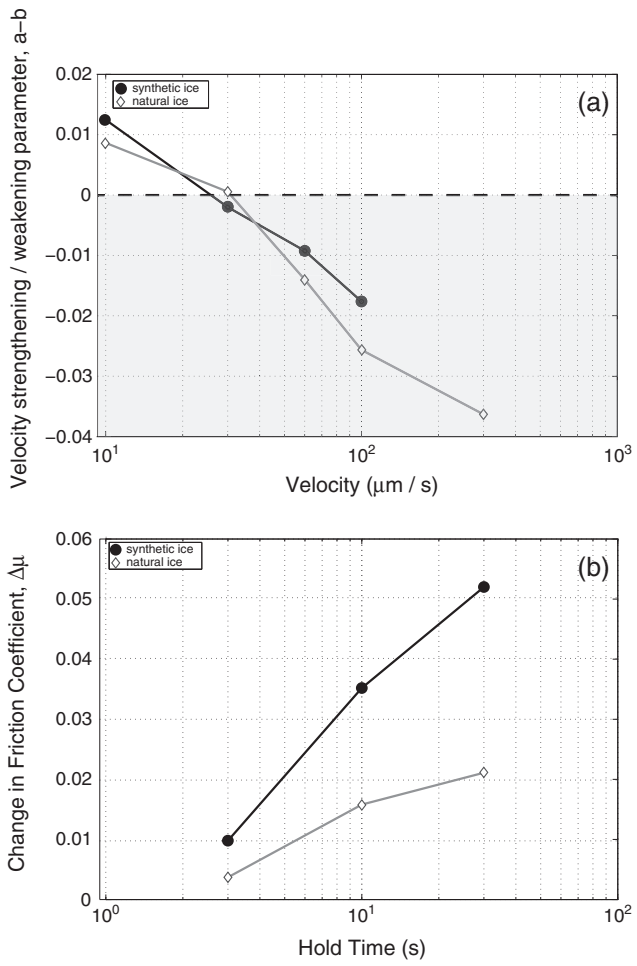

Figure 9. Comparison of friction constitutive parameters for natural versus synthetic ice. All data are for debris concentration of 16% by weight and temperature of –3°C. (a) Values of $a-b$ as a function of sliding velocity. Note that the natural and synthetic samples show the same values of $a-b$ and the same transition from velocity strengthening at low velocity to velocity weakening above a critical velocity. (b) Frictional healing data as a function of sliding velocity. Note that the natural and synthetic samples show similar values of healing and healing rate, with some variation at hold times of 30 s.

4. Discussion

[32] The unstable sliding that produces stick-slip behavior and earthquakes may arise from many physical processes, including breakage of asperities, melting of asperity contacts to lubricate them, and lubrication of asperity contacts from other sources. All of our results can be explained by a model in which (1) friction is controlled by the asperity contacts between clasts in ice and the rock substrate; (2) heating from friction at these contacts melts adjacent ice; (3) meltwater produced by shear heating lubricates the contacts; and (4) refreezing of meltwater ("freezing on") is the main source of frictional healing.

[33] Physically, for debris-free ice moving over rock, premelting [*Dash et al.*, 2006] near the melting point and true melting at the melting point produce lubricating water. When the substrate is smooth, the friction coefficient is very low [e.g., *Weertman*, 1957]. At or near the pmp, resistance to sliding of ice over rock is thus produced either by roughness on the rock, or friction from clasts in the ice [*Rabinowicz*, 1951; *Li et al.*, 2011; *Cuffey and Paterson*, 2010]. As expected from this understanding, we observe that stable sliding friction μ_{ss} increases with debris concentration, and thus increases with increasing area of clast-substrate contact and with decreasing area of ice-substrate contact. As debris increases, a greater friction coefficient μ_{ss} likely arises due to the transfer of normal stress from areas consisting primarily of ice-substrate contact to debris inclusions in contact with the substrate.

[34] It appears that meltwater can reduce friction by lubricating the contacts. Friction at ice/rock interface generates heat, which warms the substrate and clasts, which in turn warm subfreezing ice to the pmp and then melt ice. A reasonable assumption for many short-lived experiments is that nearly all the heat generated goes into melting ice. However, the frictional experiments extended for order of $t = 100$ s or longer, and with thermal diffusivity of $D \sim 10^{-6}$ m^2 s^{-1} and a diffusion distance of $\sqrt{Dt}$, the typical diffusion distance is ~ 10 mm, much larger than the region melted. Thus, the heat used in warming ice is substantial and accounts for the differential melt rates.

[35] One implication of this physical understanding is that melting, and thus lubrication, should increase with initial temperature. We observe that the friction coefficient is very low in all of the pmp experiments on Westerly Granite, rising with decreasing temperature. Temperature does affect ice deformation and other physical processes; however, our data indicate a dominant role for meltwater generation. This is supported by our observation that when we switch the pmp-experiment substrate to allow meltwater drainage, the friction coefficient is much higher (Figure 4).

[36] Recall that the friction evolution effect b describes the extent to which contact junctions weaken at the higher slip rate. Faster sliding may change the frictional interface to increase lubrication through melting, asperity breakage, or in other ways. If we think in terms of a stress boundary condition, rather than the displacement-rate boundary condition as applied in our experiments, these weakening effects would allow the original stress to sustain a higher slip velocity.

[37] A velocity perturbation on an initially well-lubricated interface will generate relatively little additional lubrication, favoring velocity-strengthening behavior. All of our pmp experiments on Westerly Granite had low stable sliding friction and were velocity-strengthening, as expected. The drained pmp experiment can allow a much larger relative increase in lubrication if the meltwater generation from a velocity step overwhelms the drainage capacity, and indeed, that experiment showed stable sliding with a high friction coefficient at slow driving velocity, but transitioned to strongly unstable sliding with increasing sliding velocity (Figure 8).

[38] All of our other experiments showed a transition from stable to potentially unstable sliding with increasing sliding velocity. The warmer subfreezing experiments, and those with more debris, can generate more meltwater and thus generate a larger change in lubrication from a given velocity perturbation. This is consistent with the observation

that the transition to unstable sliding occurs at lower driving velocity for dirtier and warmer ice.

[39] For healing, experiments at the pmp might experience various chemical or physical processes at the asperity contacts, but will have little or no freezing of meltwater. The very low rate of interface strengthening in these experiments (Figure 4) indicates that refreezing and not clast-substrate interaction is responsible for healing at colder temperatures. Healing is greater at –3°C than at –6°C, likely because more meltwater is available to refreeze (Figure 6). The log-linear dependence of healing on hold time is consistent with healing inferred by *Zoet et al.* [2012], in which seismic magnitude increased with hold time (or inter-event time) for repeating ruptures (∼25 min inter-event) of an Antarctic outlet glacier modulated by ocean tides.

[40] The experiments with natural glacial ice showed similar stability characteristics to those with laboratory ice, suggesting that the results here can be applied to real glaciers. However, the natural ice showed lower healing. We did not conduct chemical analyses on the natural ice, but its long-term interaction with entrained debris likely means that the natural ice had more impurities, which inhibit refreezing, than our laboratory samples.

[41] Our data also show that some known physical processes are not dominant under the conditions studied. These include the effect of melting on clast-substrate contact pressure, and the effects of regelation re-entrainment on healing.

[42] Melting of debris-laden ice increases the contact pressure between clasts and substrate. Here, the loss of volume from melting at the interface, or any drainage of water away from the site of melting, should lower the local pressure. The ice moves downward into the low-pressure region by creep or regelation (pressure-driven melt-refreezing) around the clast [*Hallet*, 1979, 1981], as verified by *Byers et al.* [2012]. Faster motion generates larger (drag) force on the clast, and thus larger force of the clast on the bed. This increases the stable sliding friction, which serves as a stabilizing feedback to a localized velocity perturbation. Yet, we find unstable sliding under appropriate conditions, showing that the lubricating effect of the meltwater dominates over this enhanced drag-induced friction.

[43] The heat generated during slip events releases debris as well as water. During a slip event, accumulation of thawed debris between ice and substrate may increase the number of active slip planes, allowing motion between debris and substrate or within debris as well as between debris and ice. After a slip event, the debris can be reincorporated through regelation [*Alley et al.*, 1997; *Iverson*, 1993; *Iverson and Semmens*, 1995], removing possible slip planes and thus strengthening the interface. Physically, this healing mechanism should be fastest in the warmest samples, because meltwater flow is required for regelation, and enhanced creep increases with temperature. Yet, the strengthening rate for –6°C is ∼ 6× that at the pmp, and the strengthening rate for –3°C is ∼ 11× that at the pmp. Because pmp healing is very small compared to the colder experiments, we argue that the effect of re-entrainment must be minor at most.

[44] In summary, we have not found other hypotheses that explain our observations. The data suggest a model in which friction arises almost entirely from clast-substrate interaction, heat from this interaction melts adjacent ice, and the resultant meltwater lubricates the clast-substrate contacts. Under appropriate conditions, the change in lubrication from a velocity perturbation is large enough to cause unstable sliding. Healing between slip events occurs primarily by refreezing of the meltwater.

5. Implications

5.1. Tectonic Implications

[45] In principle, any fault cutting heterogeneous material in which the asperities have a higher melting temperature than the surroundings may behave similarly to our experiments. In practice, we are probably very close to an end member of possible behavior, because of the very large difference in melting temperature between ice and rock.

[46] We note that macroscopic models of tectonic fault behavior often specify a velocity-weakening interface without treating the microphysics responsible for the instability. Thus, the rate-weakening in our experiments motivates continuing interpretation of glacier behavior within the framework of fault mechanics.

5.2. Glaciological Implications

[47] Our experiments were run at effective pressures and sliding velocities within the range observed for natural glaciers, although toward the high end, and at debris concentrations and temperatures that represent most glacier beds, using materials found in at least some glacier beds. The exclusion of grains larger than $\sim \frac{1}{10}$ of the minimum dimension allows scaling relations to be maintained, so that a small percentage of the debris concentration was not able to dominate the drag signal of the system due to limitations of sample size. All suites of experiments produced both stable and unstable sliding, with the transition to instability favored by increasing sliding velocity, increasing debris concentration, and increasing drainage in the presence of excess water.

[48] Field studies on glaciers and ice sheets often observe seismic events with source parameters consistent with glacier motion on a fault plane indistinguishable from the glacier bed [*Anandakrishnan and Bentley*, 1993]. Based on physical understanding and observations in tunnels [*Hubbard*, 2002], these subglacial events most likely are caused by stick-slip motion between debris-bearing ice and a bedrock substrate (reviewed by *Zoet et al.* [2013]). However, the resolution of seismic data precludes distinguishing between events just above, at, or just below such an interface. Our results demonstrate unstable sliding of debris-laden ice moving over bedrock, supporting that interpretation for the glacial events.

[49] On David Glacier, Antarctica, *Zoet et al.* [2012] observed transitions between aseismic or sparsely seismic motion and motion with highly repeating icequakes. Such a change is consistent with a shift in the debris concentration of the basal ice moving over an asperity, although changes in drainage or in sliding velocity, perhaps linked to filling and draining of nearby subglacial lakes [*Smith et al.*, 2009], could also be involved.

[50] Our data show only stable sliding for undrained pmp beds, but unstable behavior for subfreezing conditions. Many mountain glaciers are temperate, with the ice as well

as the basal interface at the pmp, and many of these rest on relatively impermeable bedrock. However, unstable sliding may still be possible. First, at least some regions of glacier beds typically have grooves, striae, fractures, and other features that provide sufficient connection to an active, low-pressure water system to provide drainage through channels or cavities [*Cuffey and Paterson*, 2010]. Second, large fluctuations in pressure are typically observed beneath glaciers at many time and space scales [e.g., *Murray and Clarke* [1995]; *Cuffey and Paterson* [2010]], changing the pressure melting point to favor freezing in some regions and thawing in others. In turn, it is likely that a glacier exhibiting stick-slip motion will experience interface strengthening by freeze-on in at least some places during the "stick" phase. The rich literature on glacier-bed processes suggests that study of the heterogenous local drainage and local variations in pmp will reveal a wide range of conditions, and it seems likely that some will be consistent with stick-slip behavior.

[51] The onset of stick-slip motion beneath glaciers likely speeds erosion compared to smooth sliding [*Zoet et al.*, 2013]. The results here indicate that stick-slip motion is favored by high basal shear stress, contributing to high sliding velocity, and by high debris load. For undrained beds, cold ice above the interface may favor stick-slip behavior by conducting heat away from the interface, causing restrengthening through refreezing.

6. Conclusions

[52] Laboratory experiments show that debris-laden ice can slide stably or unstably over a rock substrate. Friction generated at clast-substrate contacts heats adjacent ice, producing meltwater that lubricates those contacts. Unstable sliding is favored by high driving velocity and high debris load, both favoring rapid meltwater production in response to a velocity increase, and low initial lubrication produced by either drained or cold conditions. Healing behavior during "stick" intervals arises primarily from refreezing of meltwater, and is very small in the absence of refreezing. The experiments reported here are representative of natural glaciers, suggesting that stick-slip behavior is common from motion of debris-laden glacier ice over well-drained bedrock.

[53] **Acknowledgments.** This research was funded by the Office of Polar Programs, US National Science Foundation (NSF 0424589). Partial support provided by the US National Science Foundation through grants 0424589, 0538195, 0852697, 0907178 and 0944286), and the Sloan Program. We are grateful for discussions and comments with the Penn State Ice Group, field assistance from Knut Christianson, and laboratory assistance from Lana Zoet and Peter Burkett. The initial design and implementation was greatly aided by input and assistance from Matt Ikari.

References

Alley, R. B. (1993), In search of ice-stream sticky spots, *J. Glaciol.*, *39*(133), 447–454.

Alley, R. B., K. Cuffey, E. Evenson, J. Strasser, D. Lawson, and G. Larson (1997), How glaciers entrain and transport basal sediment: Physical constraints, *Quat. Sci. Rev.*, *16*(9), 1017–1038.

Anandakrishnan, S., and R. B. Alley (1994), Ice stream C, Antarctica, sticky spots detected by micro-earthquake monitoring, *Ann. Glaciol.*, *20*(1), 183–186.

Anandakrishnan, S., and R. B. Alley (1997a), Stagnation of ice stream C, West Antarctica by water piracy, *Geophys. Res. Lett.*, *24*(3), 265–268.

Anandakrishnan, S., and R. B. Alley (1997b), Tidal forcing of basal seismicity of ice stream C, West Antarctica, observed far inland, *J. Geophys. Res.*, *102*, 1–15.

Anandakrishnan, S., and C. Bentley (1993), Micro-earthquakes beneath Ice Streams B and C, West Antarctica: observations and implications, *J. Glaciol.*, *39*(133), 455–462.

Beeler, N. M., T. E. Tullis, and J. D. Weeks (1994), The roles of time and displacement in the evolution effect in rock friction, *Geophys. Res. Lett.*, *21*(18), 1987–1990.

Beeler, N. M., T. E. Tullis, and D. L. Goldsby (2008), Constitutive relationships and physical basis of fault strength due to flash heating, *J. Geophys. Res.*, *113*(B1), B01,401, doi:10.1029/2007JB004988.

Blankenship, D. D., C. Bentley, S. Rooney, and R. B. Alley (1986), Seismic measurements reveal a saturated porous layer beneath an active Antarctic ice stream, *Nature*, *322*, 54–57.

Blanpied, M. L., T. E. Tullis, and J. D. Weeks (1998), Effects of slip, slip rate, and shear heating on the friction of granite, *J. Geophys. Res.*, *103*(B1), 489–511.

Bowden, F. P., and D. Tabor (2001), *The Friction and Lubrication of Solids*, Oxford University Press, New York, NY.

Byers, J., D. Cohen, and N. R. Iverson (2012), Subglacial clast/bed contact forces, *J. Glaciol.*, *58*(207), 89–98, doi:10.3189/2012JoG11J126.

Carpenter, B. M., C. Marone, and D. M. Saffer (2011), Weakness of the San Andreas fault revealed by samples from the active fault zone, *Nat. Geosci.*, *4*(4), 251–254, doi:10.1038/NGEO1089.

Christianson, K. (2012), Geophysical exploration of glacier basal processes and grounding line dynamics, PhD Thesis, pp. 1–142.

Cuffey, K. M., and W. S. B. Paterson (2010), *The Physics of Glaciers, Fourth Edition*, 4th ed., Academic Press, Burlington.

Danesi, S., S. Bannister, and A. Morelli (2007), Repeating earthquakes from rupture of an asperity under an Antarctic outlet glacier, *Earth Planet. Sci. Lett.*, *253*(1-2), 151–158, doi:10.1016/j.epsl.2006.10.023.

Dash, J., A. Rempel, and J. Wettlaufer (2006), The physics of premelted ice and its geophysical consequences, *Rev. Mod. Phys.*, *78*(3), 695–741, doi:10.1103/RevModPhys.78.695.

Dieterich, J. (1978), Time-dependent friction and the mechanics of stick-slip, *Pure Appl. Geophys.*, *116*(4), 790–806.

Dieterich, J. (1979a), Modeling of rock friction. 1. Experimental results and constitutive equations, *J. Geophys. Res.*, *84*(B5), 2161–2168.

Dieterich, J. (1979b), Modeling of rock friction. 2. Simulation of preseismic slip, *J. Geophys. Res.*, *84*(B5), 2169–2175.

Dieterich, J. (1981), Constitutive properties of faults with simulated gouge, *Geophys. Monogr. Ser.*, *24*, 103–120.

Dieterich, J., and B. Kilgore (1994), Direct observation of frictional contacts: New insights for state-dependent properties, *Pure Appl. Geophys.*, *143*(1), 283–302.

Ekstrom, G., M. Nettles, and V. Tsai (2006), Seasonality and increasing frequency of Greenland glacial earthquakes, *Science*, *311*(5768), 1756–1758, doi:10.1126/science.1122112.

Emerson, L., and A. Rempel (2007), Thresholds in the sliding resistance of simulated basal ice, *The Cryosphere*, *1*(1), 11–19, doi:10.5194/tc-1-11-2007.

Fischer, U., and G. Clarke (1997), Stick slip sliding behaviour at the base of a glacier, *Ann. Glaciol.*, *24*, 390–396.

Fortt, A. L., and E. M. Schulson (2009), Velocity-dependent friction on Coulombic shear faults in ice, *Acta Mater.*, *57*(15), 4382–4390, doi:10.1016/j.actamat.2009.06.001.

Goodman, D., G. King, D. Millar, and G. Robin (1979), Pressure-melting effects in basal ice of temperate glaciers: Laboratory studies and field observations under Glacier d'Argentiere, *J. Glaciol.*, *23*(89), 259–271.

Hallet, B. (1979), A theoretical model of glacial abrasion, *J. Glaciol.*, *23*(89), 39–50.

Hallet, B. (1981), Glacial abrasion and sliding: Their dependence on the debris concentration in basal ice, *Ann. Glaciol.*, *2*(1), 23–28.

Hubbard, B. (2002), Direct measurement of basal motion at a hard-bedded, temperate glacier: Glacier de Tsanfleuron, Switzerland, *J. Glaciol.*, *48*(160), 1–8, doi:10.3189/172756502781831610.

Ikari, M. J., D. M. Saffer, and C. Marone (2009), Frictional and hydrologic properties of clay-rich fault gouge, *J. Geophys. Res.*, *114*(B5), 1–18, doi:10.1029/2008JB006089.

Iverson, N. R. (1993), Regelation of ice through debris at glacier beds: Implications for sediment transport, *Geology*, *21*(6), 559–562.

Iverson, N. R., and B. Petersen (2011), A new laboratory device for study of subglacial processes: Ffirst results on icebed separation during sliding, *J. Glaciol.*, *57*(206), 1135–1146, doi:10.3189/002214311798843458.

Iverson, N. R., and D. Semmens (1995), Intrusion of ice into porous media by regelation: A mechanism of sediment entrainment by glaciers, *J. Geophys. Res.*, *100*(B6), 10,219.

Iverson, N. R., D. Cohen, T. Hooyer, U. Fischer, M. Jackson, P. Moore, G. Lappegard, and J. Kohler (2003), Effects of basal debris on glacier flow, *Science*, *301*(5629), 81–84, doi:10.1126/science.1083086.

Karner, S. L., and C. Marone (2001), Frictional restrengthening in simulated fault gouge: Effect of shear load perturbations, *J. Geophys. Res.*, *106*(B9), 19–319–19–337.

Kirkenbride, M. (2002), 6 – Processes of glacial transportation, in *Modern and Past Glacial Environments*, pp. 1–24, Butterworth-Heinemann, Woburn, MA.

Li, Q., T. E. Tullis, D. Goldsby, and R. W. Carpick (2011), Frictional ageing from interfacial bonding and the origins of rate and state friction, *Nature*, *480*(7376), 233–236, doi:10.1038/nature10589.

Marone, C. (1998a), Laboratory-derived friction laws and their application to seismic faulting, *Annu. Rev. Earth Planet. Sci.*, *26*(1), 643–696.

Marone, C. (1998b), The effect of loading rate on static friction and the rate of fault healing during the earthquake cycle, *Nature*, *391*(6662), 69–72.

Marone, C., and B. Kilgore (1993), Scaling of the critical slip distance for seismic faulting with shear strain in fault zones, *Nature*, *362*(15), 618–620.

Marone, C., M. Cocco, E. Richardson, and E. Tinti (2009), The critical slip distance for seismic and aseismic fault zones of finite width, *Int. Geophys.*, *94*, 135–162, doi:10.1016/S0074-6142(08)00006-5.

Murray, T., and G. Clarke (1995), Black-box modeling of the subglacial water system, *J. Geophys. Res.*, *100*, 10–10.

Neave, K., and J. Savage (1970), Icequakes on the Athabasca glacier, *J. Geophys. Res.*, *75*(8), 1351–1362.

Nettles, M., et al. (2008), Step-wise changes in glacier flow speed coincide with calving and glacial earthquakes at Helheim Glacier, Greenland, *Geophys. Res. Lett.*, *35*(24), L24,503, doi:10.1029/2008GL036127.

O'Neel, S., C. F. Larsen, N. Rupert, and R. Hansen (2010), Iceberg calving as a primary source of regional-scale glacier-generated seismicity in the St. Elias Mountains, Alaska, *J. Geophys. Res.*, *115*(F4), doi:10.1029/2009JF001598PG1-12.

Peters, L. E., S. Anandakrishnan, R. B. Alley, J. P. Winberry, D. E. Voigt, A. M. Smith, and D. L. Morse (2006), Subglacial sediments as a control on the onset and location of two Siple Coast ice streams, West Antarctica, *J. Geophys. Res.*, *111*(B1), 1–14, doi:10.1029/2005JB003766.

Rabinowicz, E. (1951), The nature of the static and kinetic coefficients of friction, *J. Appl. Phys.*, *22*, 1373–1379.

Rathbun, A., C. Marone, R. B. Alley, and S. Anandakrishnan (2008), Laboratory study of the frictional rheology of sheared till, *J. Geophys. Res.*, *113*, F 000,815, doi:10.1029/2007JF000815.

Rice, J. R. (1983), Constitutive relations for fault slip and earthquake instabilities, *Pure Appl. Geophys.*, *121*(3), 443–475.

Rignot, E., J. Mouginot, and B. Scheuchl (2011), Ice flow of the Antarctic ice sheet, *Science*, *333*(6048), 1427–1430, doi:10.1126/science.1208336.

Robin, G. (1976), Is the basal ice of a temperate glacier at the pressure melting point?, *J. Glaciol.*, *16*(74), 183–196.

Rubin, A. M. (2011), Designer friction laws for bimodal slow slip propagation speeds, *Geochem. Geophys. Geosyst.*, *12*(4), Q04,007, doi:10.1029/2010GC003386.

Ruina, A. (1983), Slip instability and state variable friction laws, *J. Geophys. Res.*, *88*(10), 359–10.

Scholz, C. H. (1998), Earthquakes and friction laws, *Nature*, *391*(6662), 37–42.

Scholz, C. H. (2002), *The Mechanics of Earthquakes and Faulting*, Cambridge Univ Press, Cambridge.

Smith, A. M. (2006), Microearthquakes and subglacial conditions, *Geophys. Res. Lett.*, *33*(24), L24,501, doi:10.1029/2006GL028207.

Smith, B., H. A. Fricker, I. Joughin, and S. Tulaczyk (2009), An inventory of active subglacial lakes in Antarctica detected by ICESat (2003–2008), *J. Glaciol.*, *55*(192), 573–595, doi:10.3189/002214309789470879.

Stuart, G., T. Murray, A. Brisbourne, P. Styles, and S. Toon (2005), Seismic emissions from a surging glacier: Bakaninbreen, Svalbard, *Ann. Glaciol.*, *42*, 151–157, doi:10.3189/172756405781812538.

Tulaczyk, S., W. Kamb, and H. Engelhardt (2000), Basal mechanics of ice stream B, West Antarctica 1. Till mechanics, *J. Geophys. Res.*, *105*(B1), 463–481.

Walter, F., N. Deichmann, and M. Funk (2008), Basal icequakes during changing subglacial water pressures beneath Gornergletscher, Switzerland, *J. Glaciol.*, *54*(186), 511–521, doi:10.3189/002214308785837110.

Walter, J. I., E. E. Brodsky, S. Tulaczyk, S. Y. Schwartz, and R. Pettersson (2011), Transient slip events from near-field seismic and geodetic data on a glacier fault, Whillans Ice Plain, West Antarctica, *J. Geophys. Res.*, *116*(F1), F01,021, doi:10.1029/2010JF001754.

Weaver, C., and S. Malone (1979), Seismic evidence for discrete glacier motion at the rock-ice interface, *J. Glaciol.*, *23*(89), 171–184.

Weertman, J. (1957), On the sliding of glaciers, *J. Glaciol.*, *3*, 33–38.

West, M., C. Larsen, M. Truffer, S. O'Neel, and L. Leblanc (2010), Glacier microseismicity, *Geology*, *38*(4), 319–322, doi:10.1130/G30606.1.

Wiens, D. A., S. Anandakrishnan, J. P. Winberry, and M. A. King (2008), Simultaneous teleseismic and geodetic observations of the stick–slip motion of an Antarctic ice stream, *Nature*, *453*(7196), 770–774, doi:10.1038/nature06990.

Winberry, J. P., S. Anandakrishnan, and R. B. Alley (2009a), Seismic observations of transient subglacial water-flow beneath MacAyeal Ice Stream, West Antarctica, *Geophys. Res. Lett.*, *36*(11), 1–5, doi:10.1029/2009GL037730.

Winberry, J. P., S. Anandakrishnan, R. B. Alley, R. A. Bindschadler, and M. A. King (2009b), Basal mechanics of ice streams: Insights from the stick-slip motion of Whillans Ice Stream, West Antarctica, *J. Geophys. Res. Earth Surf.*, *114*, F01,016, doi:10.1029/2008JF001035.

Zoet, L. K., S. Anandakrishnan, R. B. Alley, A. A. Nyblade, and D. A. Wiens (2012), Motion of an Antarctic glacier by repeated tidally modulated earthquakes, *Nat. Geosci.*, *5*(9), 623–626, doi:10.1038/NGEO1555.

Zoet, L. K., R. B. Alley, S. Anandakrishnan, and K. Christianson (2013), Accelerated subglacial erosion in response to stick-slip motion, *Geology*, *41*(2), 159–162, doi:10.1130/G33624.1.